ELSEVIER

Journal of Nuclear Materials 290–293 (2001) 1144–1147

journal of nuclear materials

www.elsevier.nl/locate/jnucmat

Measurement of thermal wall-load distribution caused by the locked mode in a reversed-field pinch plasma

Y. Yagi [a,*], S. Sekine [a], H. Koguchi [a], T. Bolzonella [b], H. Sakakita [a]

[a] *Electrotechnical Laboratory, Energy Technology Division, AIST, 1-1-4 Umezono, Tsukuba-shi, Ibaraki, 305-8568 Japan*
[b] *Consorzio RFX, Corso Stati Uniti 4, 35127 Padova, Italy*

Abstract

Spatially localized heat flux due to the locked mode in a reversed-field pinch device, TPE-RX, is investigated by using a multipoint vessel temperature monitoring system (VTMS) which has 268 thermocouples distributed on the outer surface of the vessel system. It is shown by two-dimensional mapping that the locally enhanced thermal wall load correlates closely with the mode locking positions. Heat flux shows spatial peaks (full width at half maximum) of $\sim 10^\circ$ and $\sim 100^\circ$ in the toroidal and poloidal directions, respectively. Typical heat flux at the locked position is estimated to be of the order of 100 MW/m^2, and the increment of the vessel temperature on the plasma side-surface exceeds 1000° with 0.35 MA plasma current.

Keywords: Thermal load; Reversed field pinch; Locked mode

1. Introduction

In tokamak and reversed-field pinch (RFP) plasmas, a peaked-heat flux to the first wall arises from the shift of the equilibrium position, the existence of the error field and perturbed magnetic field due to plasma instabilities. Equilibrium and error field can be optimized or minimized by means of external field control. On the other hand, the control of plasma instabilities is difficult and needs feedback control for sophisticated coil systems.

In RFP plasmas, mode locking phenomena are often observed. The locked mode is a magnetohydrodynamic instability which has a spatially enhanced magnetic structure (phase-locked structure) which remains at the same place in time (wall-locked). The phase-locked structure forms a helical distortion of the last closed flux surface (LCFS), which was originally called the 'slinky' structure [1,2]. In large-sized RFPs, a typical locked mode has been observed in RFX [3], and rotation and wall-locking of the phase-locked structure has been observed in MST [4]. These mode locking phenomena in RFP plasmas cause a peaked-heat flux because of its spatially localized and stationary nature. This paper presents a two-dimensional correlation between the estimated heat flux and a magnetic structure of the locked mode in another large RFP device, TPE-RX [5,6]. Our previous study [7] showed that typical mode locking discharges exist in TPE-RX. In the present study, the data from the vessel temperature monitoring system (VTMS) [8] is fully analyzed, and a two-dimensional comparison between the heat flux distribution and the magnetic deformation is made. In particular, the absolute value of the heat flux distribution, degree of peakedness of the heat flux, and spatial correlation with shift of the LCFS for the typical mode locking discharges in TPE-RX are presented.

2. Experimental device and the vessel temperature monitoring system

TPE-RX ($R/a = 1.72/0.45$ m, R and a are the major and minor radii, respectively) is characterized by a close-

* Corresponding author. Tel.: +81-298 61 5769; fax: +81-298 61 5754.
E-mail address: yagi@etl.go.jp (Y. Yagi).

0022-3115/01/$ - see front matter
PII: S0022-3115(00)00551-1

fitting multilayered shell structure with full equilibrium controlling capability up to $I_p = 1$ MA. The center of the vacuum vessel is shifted outward from the thick shell so that no DC vertical field was applied in the discharges studied here to have the LCFS matched with the limiter circumference [5,6]. The vacuum vessel is made from stainless steel of type 316L and consists of 16 bellows sections (2 mm thick) and 16 port sections (6 mm thick). The mushroom-shaped molybdenum limiters (98.5 mm diameter, a total number of 244 pieces) are installed on the inside surface of the port sections to protect the adjacent bellows by protruding 5 mm from the bellows.

Magnetic coils and thermocouples (TCs), which forms the VTMS, are installed on the surface of the vacuum vessel. They are distributed to form the arrays to analyze the distribution of the vessel surface temperature and the temporal evolution of the magnetic signals, respectively. The VTMS consists of 268 thermocouples (chromel-constantan type), extension wires and a stand-alone controlling/monitoring system [8]. The TCs are distributed around the torus to measure the toroidal and poloidal distribution of the heat flux. The TCs are distributed to measure toroidal distributions on the equatorial plane and poloidal distributions at representative poloidal cross-sections, i.e., poloidal shell gaps of the shell layers and normal sections with no gaps. In particular, the TCs are densely distributed at the toroidal angle, ϕ, in the range of 120–240° where the poloidal gap of the thick shell exists at $\phi = 180°$. Note that the locked mode occurs at the thick shell gap with a larger probability (18–26%) than at the other toroidal locations [7]. Fig. 1(a) shows the map of the TCs at $\phi = 120$–$240°$ in the rectangular plane of ϕ–θ, where θ is the poloidal angle defined to be $\theta = 0$ on the outboard side of the equatorial plane. The TCs are attached to three parts of the vessel structure (Fig. 1(b)); on the outside surface of the bellows valley ($r = 457$ mm), at the bellows peak ($r = 484$ mm), and on the port section ($r = 482$ mm). The location at the bellows valley is most sensitive to local heat flux because of the thinness of the wall.

All signals from the TCs are simultaneously sampled every 0.5 s and stored in a data file. After the end of each discharge, the vessel temperature reaches its peak characteristically in approximately 10–15 and 100–150 s for the bellows valley and peak, respectively [8]. The temperature increment at the bellows valley on the outboard side of the equatorial plane ranges from 10° to 40° at the peak of the mode locking position. On the other hand, the temperature increment at the port section is very small (typically 0.3–2°) and does not show a systematic temporal evolution. Because of this, the data only from the bellows section are used in the next section to evaluate input heat flux and vessel temperature on the plasma side.

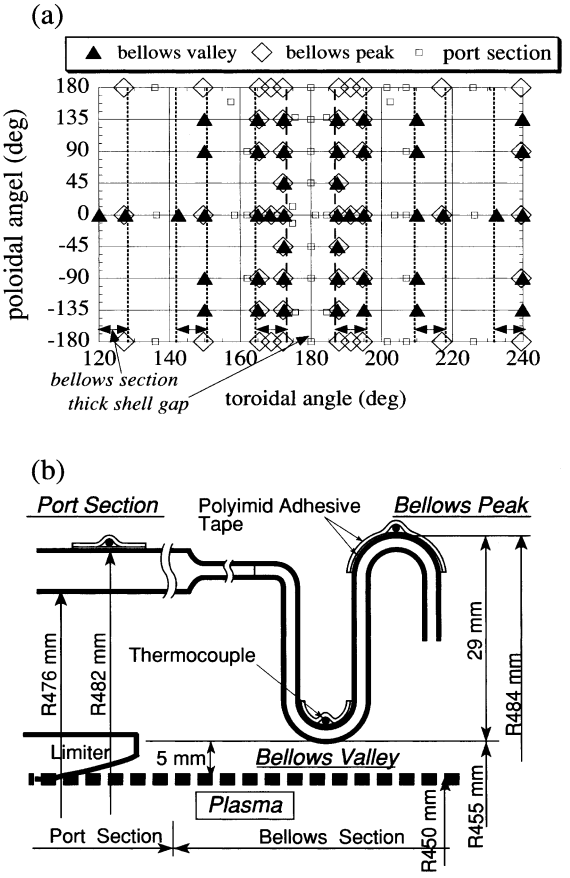

Fig. 1. Location mapping of the TCs (a) at the region near the thick shell gap and (b) in the three kinds of vessel surface where TCs are attached. The three marks – solid triangle, diamond, and square – correspond to the TC locations at the bellows valley, bellows peak and the port section, respectively.

3. Results and discussions

We investigated a series of RFP discharges with $I_p = 0.35$ MA, p_{D_2} (filling pressure of deuterium gas) = 0.7 mTorr, F (reversal ratio) = −0.15, and Θ (pinch parameter) = 1.5, where typical locked mode is observed.

Normalized spatial profiles of the temperature increment obtained from the toroidal and poloidal arrays of the TCs at the bellows valley are plotted in Fig. 2 for two discharges. The toroidal array is selected from the TCs at the bellows valley on the outboard side of the equatorial plane, and the poloidal array closest to the mode locking position is selected for each discharge. The result shows that the vessel temperature peaked not only in the toroidal direction (Fig. 2(a)) but also in the poloidal direction (Fig. 2(b)). The typical full width at half maximum (FWHM) of the peaked profiles is ~10° and ~100° for the toroidal and poloidal directions, respectively.

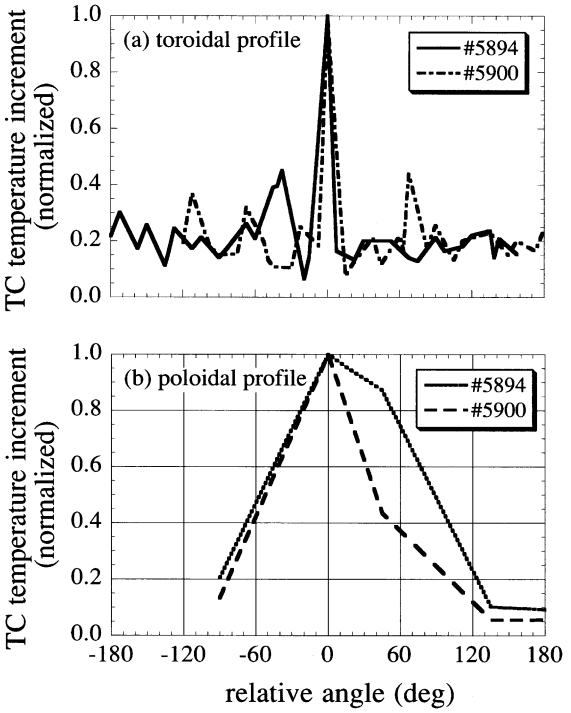

Fig. 2. (a) Toroidal and (b) poloidal profiles of the normalized TC temperature increment at the bellows valley. Results for two discharges are plotted.

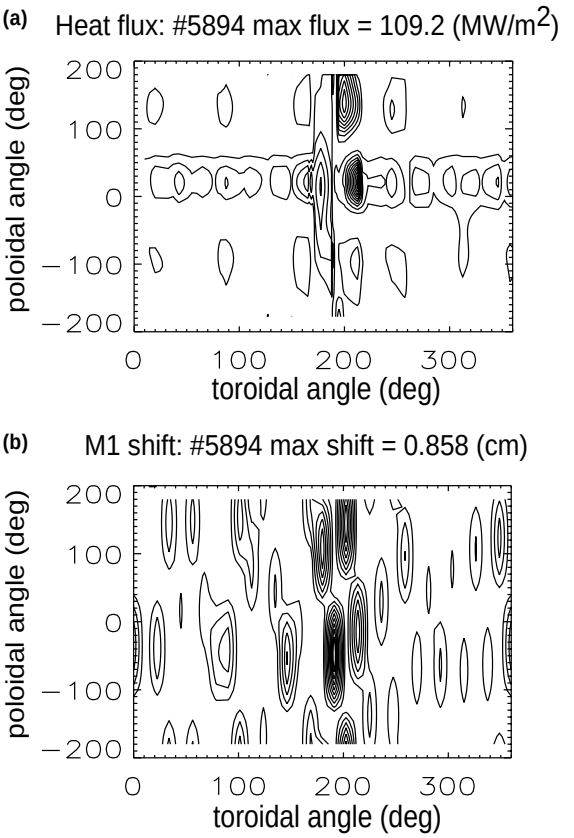

Fig. 3. (a) Contour plots of the estimated heat flux and (b) the excess shift of the LCFS beyond the limiter circumference at $a = 0.45$ m.

The heat flux at the bellows valley is estimated as follows by assuming that the heat deposited in the region $\Delta w \times \Delta L$ is diffused into the region larger by thermal diffusion length, d, in the stainless steel in the time to reach the peak ($t = 12$ s).

$$\Gamma_{\rm v}\ ({\rm W/m^2}) = \frac{\gamma}{\Delta t}\rho C f_{\rm v} d \Delta T_{\rm v} \approx 5 \times 10^6 \Delta T_{\rm v}\ ({\rm deg}). \qquad (1)$$

For the bellows peak, the heat flux is obtained by assuming that the temperature increase is due only to the heat conduction from the heat deposition to the adjacent bellows valley.

$$\Gamma_{\rm p}\ ({\rm W/m^2}) = \frac{\gamma}{\Delta t}\rho C f_{\rm p} d_0 \Delta T_{\rm p} \approx 11 \times 10^6 \Delta T_{\rm p}\ ({\rm deg}), \qquad (2)$$

where $\gamma = \sqrt{\pi e/2} = 2.07$, Δt is the pulse duration time of the discharge ($= 50$ ms), ρ the specific gravity, C the specific heat, $f_{\rm v}$ ($= 3$) an enhancement factor for the bellows valley obtained with $\Delta w = 10$ mm and $\Delta L = 2\pi a/4$, $f_{\rm p}$ ($= 6.6$) an enhancement factor for the bellows peak, d_0 the thickness of the bellows ($= 2$ mm), $\Delta T_{\rm v}$ the temperature increment at the bellows valley at $t = 12$ s after the discharge, and $\Delta T_{\rm p}$ is the maximum temperature increment at the bellows peak. The thermal diffusion length, d, is calculated from $d = \sqrt{2t\alpha}$, where $\alpha = k/\rho C$, and k is the thermal conductivity. The values at room temperature are used for ρC and k for the stainless steel. Although they may vary with temperature, the deviation in the final result is estimated to be small.

A typical result of the heat distribution is plotted in Fig. 3(a), which is the case wherein the locked mode appears at the thick shell gap. In Fig. 3(a), the heat flux distribution is plotted as a contour map in the ϕ–θ plane covering the entire torus ($\theta = -180$–$180°$, $\phi = 0$–$360°$) in order to show if any hot spots exist at the TC locations. The contours are drawn by using a contour-plot routine for irregularly spaced data provided in IDL (Research Systems). Through the contour-plot routine, a center of the contour can appear where there is no TC, depending on the values of the TC around there. It should be noted here, however, that the contour map away from the thick shell gap region (120–240°) is essentially one-dimensional distribution on the outside surface of the equatorial plane. Also note that the lack of the TC data at the port section (see TC locations in Fig. 1(a)) may cause an apparent depletion of the heat flux if the peaked heat flux is concentrated there. In the case described in Fig. 3(a), the maximum heat flux,

110 MW/m^2, appears at $\theta = 0°$ and $\phi = 210°$. The second island with a smaller peak, 80 MW/m^2, appears at $\theta \approx 150°$ and $\phi = 200°$. These patterns are then compared with the shift of the LCFS obtained from the magnetic measurement.

From the B_r-loop coil arrays attached at the top and bottom (32 top $\times$ 32 bottom) of the vacuum vessel surface, the vertical and horizontal shift, Δ_V and Δ_H, respectively, of the LCFS are calculated at toroidal angles spaced every 11.25°, according to the formulation given in [9]. The radial protrusion of the circle-shaped LCFS from the limiter circumference ($a = 0.45$ m) is then calculated at a given poloidal angle θ. This excess protrusion of the LCFS, Δr, is plotted in Fig. 3(b) in the ϕ–θ plane for the same discharge as that of Fig. 3(a). The result reflects a typical phase-locked structure of multiple modes. Fig. 3(b) shows that Δr has large values at $\phi = 180$–$220°$, and that Δr forms some island patterns, some of which correlate with those in Fig. 3(a). The maximum Δr, 0.9 cm, appears at $\phi \approx 190°$ and $\theta \approx -50°$. We also note that Δr has apparent small islands covering approximately 90° in the poloidal direction. This pattern is partially affected by the spatial resolution of the magnetic arrays ($= 11.25°$ and 90° in the toroidal and the poloidal directions, respectively). Nevertheless, Figs. 3(a) and (b) show the patterns' close correlation. Fig. 3 shows a typical case of the mode locking discharge. Our previous study of the toroidal (one-dimensional) distribution of ΔT_v for the 100 mode locking discharges [7] showed that the toroidal position where the peak of ΔT_v appears correlates well with the place where the maximum shift appears. In the present study, we investigated two-dimensional correlation, and the result shows that some pattern of ΔT_v corresponds to that of Δr, and that the poloidal heat flux also has a peaked profile whose FWHM is approximately 100° ($\sim 2\pi a/4$).

The temperature increment at the bellows valley on the plasma-facing surface during the discharge duration can be estimated as

$$\Delta T_{pl} = f_v \sqrt{\frac{t}{\Delta t}} \Delta T_v = 46 \Delta T_v, \tag{3}$$

which gives an average value of $\Delta T_{pl} \approx 1200°$. It should be noted here that the estimated values of the heat flux and ΔT_{pl} depend on the assumption of the initial size of the area of heat deposition. The value of f_v corresponds to the case where the heat is deposited to the width of a bellows valley ($= 10$ mm) with a poloidal span of 90°.

4. Conclusion

Two-dimensional heat flux distribution of the locked mode in the TPE-RX reversed-field pinch device is evaluated using the VTMS, and the results are compared in terms of excess shift of the LCFS. The results show that both patterns have reasonable correlation, in agreement with similar studies of RFX [10,11]. The results illustrate the applicability of the VTMS for spatially localized heat deposition as studied here.

References

[1] T. Tamano, W.D. Bard, C. Chu et al., Phys. Rev. Lett. 59 (1987) 1444.
[2] G. Hedin, Plasma Phys. Control. Fus. 40 (1998) 1529.
[3] A. Buffa, F. Gnesotto, V. Antoni et al., in: Proceedings of the 21st EPS Conference on Controlled Fusion and Plasma Physics, Montpellier, 1994 (European Physics Society, Petit-Lancy, 1995), Part I, p. 458.
[4] A.F. Almagri, S. Assadi, S.C. Prager, J.S. Sarff, D.W. Kerst, Phys. Fluids B 4 (1992) 4080.
[5] Y. Yagi, S. Sekine, H. Sakakita et al., Fus. Eng. Des. 45 (1999) 409.
[6] Y. Yagi, S. Sekine, T. Shimada et al., Fus. Eng. Des. 45 (1999) 421.
[7] Y. Yagi, H. Koguchi, H. Sakakita et al., Phys. Plasmas 6 (1999) 3824.
[8] Y. Yagi, H. Sakakita, H. Koguchi, S. Sekine, Fus. Eng. Des. 46 (1999) 65.
[9] P. Zanca, S. Martini, Plasma Phys. Control. Fus. 41 (1999) 1251.
[10] M. Valisa, T. Bolzonella, L. Carraro et al., J. Nucl. Mater. 241–243 (1997) 988.
[11] P. Sonnato, P. Zaccaria, Fus. Eng. Des. 39&40 (1998) 401.